Geosynthetics, J. Kuwano & J. Koseki (eds)

A new dimensioning approach for geogrids with stiff junctions

Ziegler, M.
Geotechnical Engineering, Aachen University of Technology, Germany
ziegler@geotechnik.rwth-aachen.de

Keywords: dimensioning of geogrid reinforced constructions, drag-force distribution, mobilisation function

ABSTRACT: Construction of slopes and retaining walls as geogrid reinforced ground compounds is of increasing importance. The dimensioning of the required anchor length of the reinforcement layers is based on the results of pull-out tests. Most calculation methods act on the assumption of a linear distribution of tensile forces over the anchor length. Test results attained at RWTH Aachen University of Technology show that this approach is conservative. Based on these results a calculation model is presented with which the observed effects can be mapped to serve not only an economical dimensioning of the anchor length but also a realistic appraisal of the behaviour of a geogrid reinforced construction in the state of serviceability.

1 INTRODUCTION

Slopes and bearing constructions made of geogrid reinforced ground compounds are characterized by their adaptability to complex terrain, their economic efficiency due to little material expense, their high tolerance towards subsoil settlements as well as their high rigidity against static loads.

Numerous tests have shown that the actual safety factor of slope stability is far greater than the calculated value (e.g. Bräu, Floss 2000). The high bearing capacity cannot merely be explained by the frictional behavior between the building materials used. Apparently, additional resistance forces are mobilised in front of the cross bars.

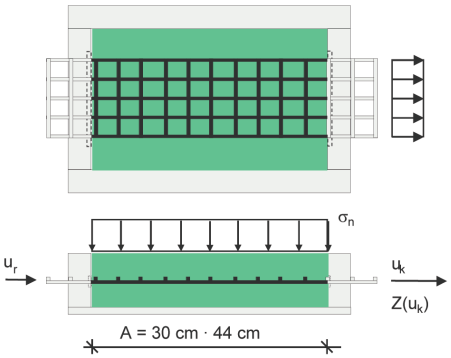

Figure 1. Experiment set-up.

2 EXPERIMENTS

A 30 cm · 44 cm modified shear box was used to conduct pull-out experiments on a geogrid of high tensile stiffness, made of polyester Secugrid 40/40 Q6 by Naue GmbH. For this purpose the upper and lower part of the shear box have been fixed, whereas the grid was pulled out by the drive of the shear test apparatus. Several samples with differing numbers of cross bars and cross bar clearance have been used. As filling soil, a very dense sand was used. Fig. 1 displays a sketch of the experiment set-up.

Figure 2 displays a characteristical test result for a grid without cross bars (S0-sample, reference test) and a grid with two cross bars (S2-samples) for pull-out distances uk at the clamp up to 50 mm for different normal-stresses.

The drag trajectories with the S2-sample clearly exceed the ones with the S0-sample. This is due to the fact that the cross bars and the filling soil in front of them contribute to the load distribution. The pull out forces are only limited for greater pull outdistances by exceeding the grid's tensile strength or junction strength.

In order to visualise the importance of cross bar bearing effects tests with steel grids with a similar geometry have been conducted (Figure 3).

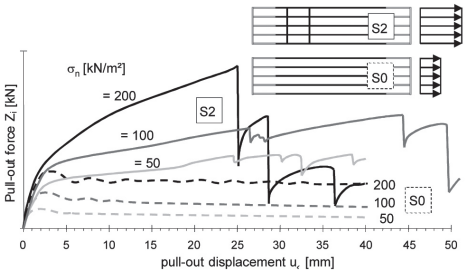

Figure 2. Typical test results.

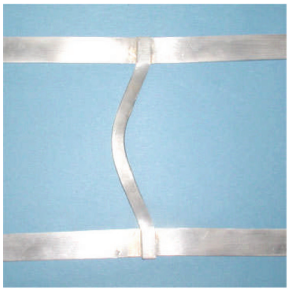

Figure 3. Permanent deformation of a welded steel specimen.

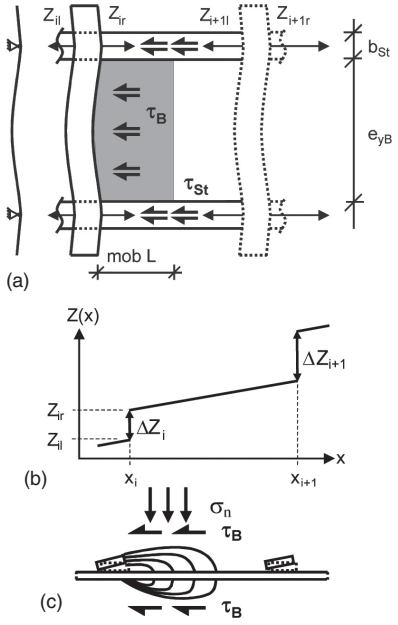

Figure 4. Mechanism of pull-out.

3 CALCULATION MODEL

The resistance of the pulled grid is induced by friction between the filling soil and the longitudinal bars and the ploughing resistance of the cross bars, respectively (Figure 4a).

The first one is considered constant for a given normal stress over the bar length leading to a linear increase of the drag force (Fig. 4b). To explain the large cross bar bearing effects observed, a mechanical model was designed in which the cross bar is being treated as a beam on two supports. By the movement of the grid, the ground particles in front of the cross bar would wedge, being pushed ahead of the cross bar as by a plough (Figure 4c).

The soil resistance affecting the cross bar is the integral of the shear stress τ_B on the contribution area which is dependant on the soil's friction angle and the locally acting normal stress σ_n:

$$E_{PQ} = \int_A \tau_B dA = \int_A \sigma_n \cdot \tan \varphi_B dA \qquad (1)$$

The soil resistance E_{pQ} in front of a cross bar i is inserted into the longitudinal bars in form of a drag force leap $\Delta Z_i = E_{pQ}$ at the grid joint.

The soil area that is actually shifted after a given pull-out displacement u_{QSt} is simplified as a coextensive rectangle measuring mob $A = e_{yB} \cdot$ mob $L(u)$ (Fig. 4a). As the normal stress applying to this area is assumed to be equally dispensed over the bar surface and the filling soil in the grid spaces, the shear stresses acting on the top and the bottom sides of the rectangle are also constant, rendering a description of the drag force leap possible:

$$\Delta Z_i = 2 \cdot \sigma_n \cdot \tan \varphi_B \cdot e_{yB} \cdot \text{mob } L(u) \qquad (2)$$

As the pull-out displacement is growing, the only changing component in this equation is mob L being a proportional scale for every cross bar's absorbed soil resistance and the drag force leap ΔZ_i.

The soil resistance resulting from the ploughing effect is considerable and is by far exceeding the interface friction between the grid and the filling soil. However, the mobilised area can grow no more as soon as it touches the neighbouring cross bar. Therefore, the bearing capacity of a single cross bar is limited by its distance to the adjacent bar. If pulled out further, the cross bars and the mobilised soil would slip through the surrounding filling soil.

The bearing capacity of single cross bars can be displayed by using the results of the pull-out experiments on S1- and S0- samples. The increase in pull-out force due to a single cross bar is $\Delta Z_i\,(u) = Z_1\,(u) - Z_0\,(u)$.

Using the proportional correlation between ΔZ_i and mob L according to (2), mob L can be determined from

$$\text{mob } L(u) = \frac{Z_1\,(u) - Z_0\,(u)}{2 \cdot \sigma_n \cdot \tan \varphi_B \cdot e_{yB}} \qquad (3)$$

for every normal stress tested. Thus mob L and also the pull out force is a function of the clamp displacement and the acting normal stress (fig. 5).

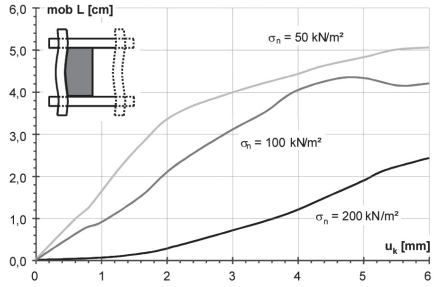

Figure 5. Mobilisation function vs. clamp displacement.

If one compares the curves at the same clamp displacement, the mobilised areas seem to decrease with increasing normal stress.

This is misleading as the reason for the granular structure's restraint is not actually the clamp displacement u_k, but the actual displacement u_{QSt} of the grid bar. The actual displacement u_{QSt} can be determined from the clamp displacement u_k and grid strain $\varepsilon_x(x)$, which can be taken from the characteristic stress-strain curve of a tensile test which is provided by the manufacturer of the grid.

$$u_{QSt}(u_k) = u_k - \int_{x_{QSt}}^{\alpha_k} \varepsilon_x(x)\,dx \qquad (4)$$

Figure 6 displays the mobilisation function vs. the true cross-bar displacement. As indicated by the arrows a clamp displacement of u_k = 6 mm causes clearly lower values of 5, 3.6 and 1.4 mm for the cross bar displacement, the lowest value being the result of the highest normal stress. The graphs of the adjusted mobilisation functions virtually coincide as a good approximation. Using a real grid the adjusted mobilisation function has to be lopped for mob $L = 4$ cm being the distance to the neighbouring cross bar.

The lower Z_0-line in Fig. 7 displays the linear drag force distribution in *S*0-grids, assuming a constant shear stress insertion into the longitudinal bars. At the rear end, the grids drag force equals zero. Thus, the drag force distribution can also be applied with the same gradient from the rear box slot upto the first cross bar. The unknown drag force leap occurring at

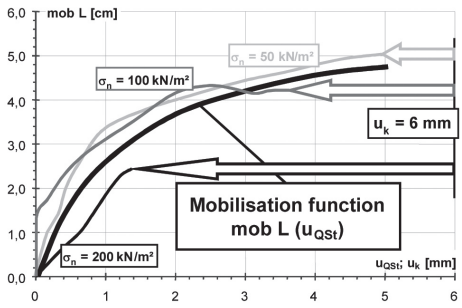

Figure 6. Mobilisation function vs. cross bar displacement.

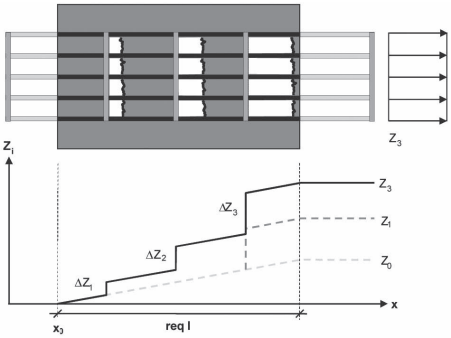

Figure 7. Drag force curve on a full grid.

the cross bar ΔZ_1 can be read off the graph as the difference between drag forces on the left and the right side of the cross bar (dashed Z_1-line in Figure 7).

In grids with more than one cross bar, the rear cross bars cause slighter drag force leaps than the ones in the front as the continuous strain of the grid diminishes the displacement of the cross bars. Thus, the cross bar's loads decrease continuously in the rear area.

This effect, which is not considered by the common design procedure, wears on up to the point x_o from which on the grid is no longer subject to significant displacement since no more loads are transferred by the cross bars. Not taking any safety factors into consideration, the distance from the place of pull-out force induction to the point x_o equals the required anchor length req l of the reinforcement.

4 DIMENSIONING NOMOGRAM

The mechanical correlations between the variables $Z(x)$, $\varepsilon_x(x)$ and $u(x)$ explained above allow for a step by step determination of these values. The following dimensioning nomogram (Fig. 8) was developed for that purpose.

The nomogram's left part represents the grid's longitudinal axis. The undetermined displacement $u(x)$ and the strain $\varepsilon_x(x)$ are displayed in the upper left, the grid drag force $Z(x)$ in the lower left part.

$Z_i(x)$ starts at zero and its gradient between the cross bars is given by the known interface shear stress. Its distribution can thus be calculated and displayed up to the first cross bar (i = 1). The according strains $\varepsilon_x(x)$ can be taken from the haracteristic geogrid stress-strain curve and are displayed in the upper left part of the nomogram. They also start at zero on the rear end of the grid.

In order to determine the grid displacement distribution $u(x)$, the strains have to be integrated with the grid front's displacement u_0 on the left end usually set to 0. This means, that the grid is subject to strain, but is not yet moved in the left end.

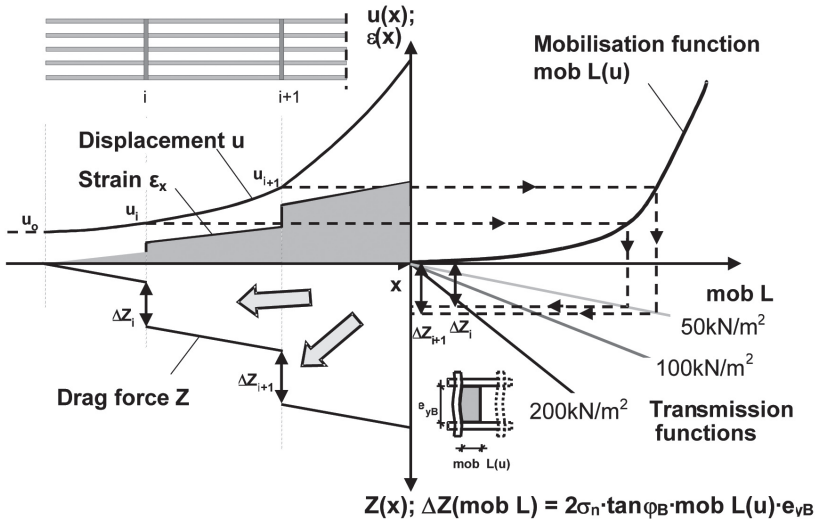

Figure 8. Dimensioning nomogram.

In the right part of the nomogram the soil mechanical correlations between the mobilised length mob L on the abscissa, the grid displacement u and the drag force leaps ΔZ are applied. In the upper right part, the specific mobilisation function is applied over the actual cross bar displacement u_{QSt}, the axes being switched in comparison to Fig. 6. In the lower right part, the transmission function graphs according to (2) are displayed, determining the drag force leap ΔZ corresponding to a given value mob L in dependence of the normal stress applied.

The displacement u_1 of the first cross bar serves as an input value for the mobilisation function. Its abscissa shows the soil area shifted by the first cross bar.Taking this mob L value, one goes down onto the graph of the transmission function corresponding to the actually occurring normal stress, reading off the respective drag force leap ΔZ_1 on the ordinate. This is attached to the drag force distribution below left. Having finished the first step of calculation, the three unknown values $\varepsilon_x(x)$, $u(x)$ and $Z(x)$ are now determined for the area between the grid front and the first cross bar.

In exactly the same way the calculations are carried out for step two of calculation to determine values $\varepsilon_x(x)$, u_2 and Z_2 up to the second cross bar. The displacement u_2 is larger than u_1. Transferring this to the mobilisation function and the fitting transmission function determines the drag force leap ΔZ_2 at the second cross bar, which turns out to be larger than ΔZ_1 at the first one as well.

To verify the experiment results, this method of calculation is repeated subsequently for every cross bar in place, until the front end of the grid or the clamp respectively is reached. If the displacement at the open grid end is preselected for a given construction situation, one can determine either the grid length for a given force to be absorbed or determine the absorbable force for a given grid length. For more details refer to Ziegler and Timmers (2004).

5 SUMMARY AND FUTURE PROSPECTS

With the calculation model presented here, it is rendered possible to use the available knowledge on the complex interaction between the reinforcement and the filling soil in a quantitative way in order to determine not only the necessary dimensions of the geogrid anchor length but also to appraise the behaviour of a geosynthetic reinforced construction in the state of serviceability.

REFERENCES

Bräu, G. and Floss, R.: Geotextile Structures used for the Reconstruction of the Motorway Munich – Salzburg. In: EuroGeo (2000), Proceedings of *the Second Europ. Geosynth. Conf.*, Bologna, Italy, 15-18 Oct. 2000.

Ziegler, M. and Timmers, V. (2004). A new approach to design geogrid reinforcement. Proceedings *of the third Europ. Geosynth. Conf.*, Munich, DGGT (2004).